Unlocking Mg^{2+} storage in imine-functionalized COF@CNTs hybrids: role of in situ coating in enhancing magnesium battery performance

Xiangming Wang,‡[a] Yang Zhao,‡[a] Han Qin,[a] Feng Yan,*[b] Tao An,[a] Weimin Liu,[a] Yu Su[a] and Xianbo Yu*[a]

[a] Key Laboratory for Photonic and Electronic Bandgap Materials, Ministry of Education, School of Physics and Electronic Engineering, Harbin Normal University, Harbin 150025, China

[b] Key Laboratory of In-Fiber Integrated Optics, Ministry of Education, College of Physics and Optoelectronic Engineering, Harbin Engineering University, Harbin 150001, China

‡ Xiangming Wang and Yang Zhao contributed equally to this work.

∗Corresponding Author E-mail: Xianbo Yu (ge_yuxianbo@126.com); Feng Yan (yanfeng@hrbeu.edu.cn)

Materials characterization

The morphology and structure of COF@CNTs were observed and analyzed by X-ray diffractometer (XRD, PANalytical X′Pert PRO), scanning electron microscope (SEM, Hitachi SU8010), and transmission electron microscope (TEM, Tecnai G2 F30), and the samples were detected by the specific surface area test (BET, ASAP 2020) to determine the Specific surface area, and the chemical composition of the samples were detected by X-ray photoelectron spectroscopy (XPS, AXIS SUPRA+) and Fourier transform infrared spectroscopy (FTIR, NICOLET 6700).

Electrochemical Measurements

The cathode was fabricated by blending the active material with polyvinylidene fluoride (PVDF) and acetylene black at a mass ratio of 8:1:1 to form a homogeneous slurry, which was then pasted onto carbon fiber paper with a mass loading of 1.0 mg cm^{-2}. In an argon-filled glove box with humidity and oxygen levels maintained below 0.1 ppm, the commercially obtained magnesium metal sheets were repeatedly polished using 2000-grit sandpaper to remove the surface MgO oxide layer. CR2025-type coin cells were subsequently assembled using the prepared cathode, a polished Mg plate as the anode, and a microporous membrane (Celgard 2400) as the separator. All-phenyl complex (APC) electrolyte for MIBs was prepared as follows: 2.133 g of aluminium chloride ($AlCl_3$) was slowly added into 24 mL of anhydrous tetrahydrofuran (THF) solution and vigorous stirring for 12 h, and then 16 mL of phenyl magnesium chloride (MgPhCl) solution in THF was added dropwise to form the APC electrolyte under vigorous stirring for another 12 h. Electrochemical impedance spectroscopy (EIS) measurements were conducted in the frequency range of 0.1 Hz to 100 kHz. Prior to conducting the *ex-situ* X-ray diffraction (XRD) analysis, the CNTs@COF-2 was carefully detached from the carbon paper following the charge-discharge cycling, then sequentially washed and centrifuged using THF and N-methylpyrrolidone (NMP). Subsequently, the materials were dried under controlled conditions and prepared for characterization.

Galvanostatic intermittent titration technique (GITT) was measured for 10 min discharge and 30min relaxing time at the current density of 20 mA g^{-1}. The diffusion coefficient (D) can be calculated by Fick' second law:

$$D = \frac{4}{\pi\tau}\left(\frac{m_b V_m}{M_b S}\right)^2\left(\frac{\Delta E_s}{\Delta E_t}\right)^2$$

where τ is the time of current pulse. V_m, m_b, and M_b represent molar volume, the mass, and molar mass of materials, respectively. S is the contact area of electrode/electrolyte. ΔE_s and ΔE_t are the steady-state potential change by the current pulse and potential change during the constant current, which are eliminated with the *IR* drop.

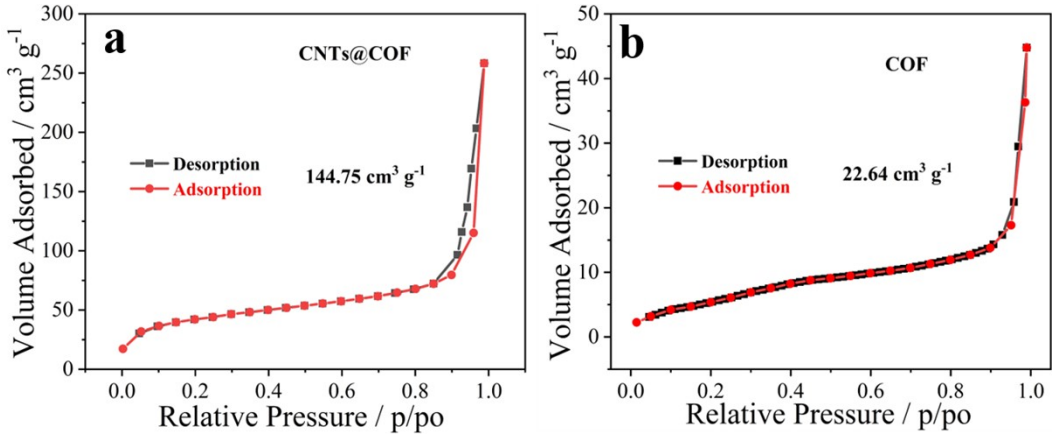

Fig. S1. Nitrogen adsorption and desorption isotherms of (a) CNTs@COF and (b) COF.

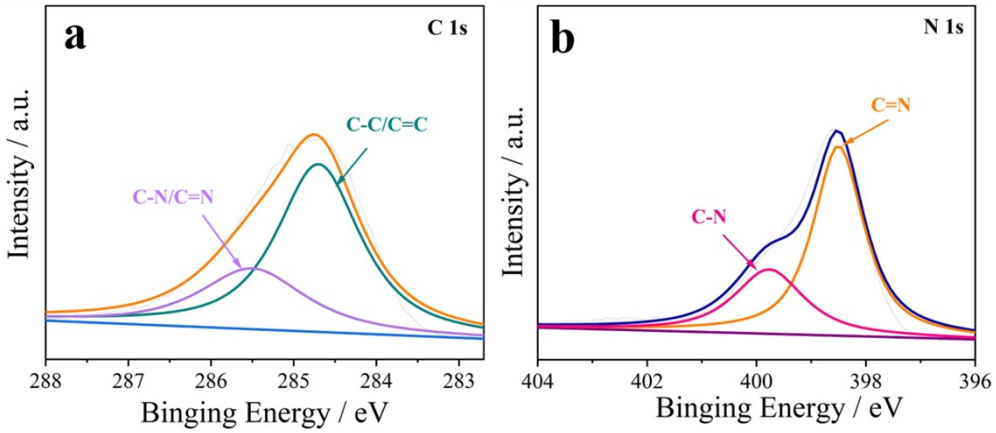

Fig. S2. XPS spectra of (a) C 1s and (b) N 1s in CNTs@COF.

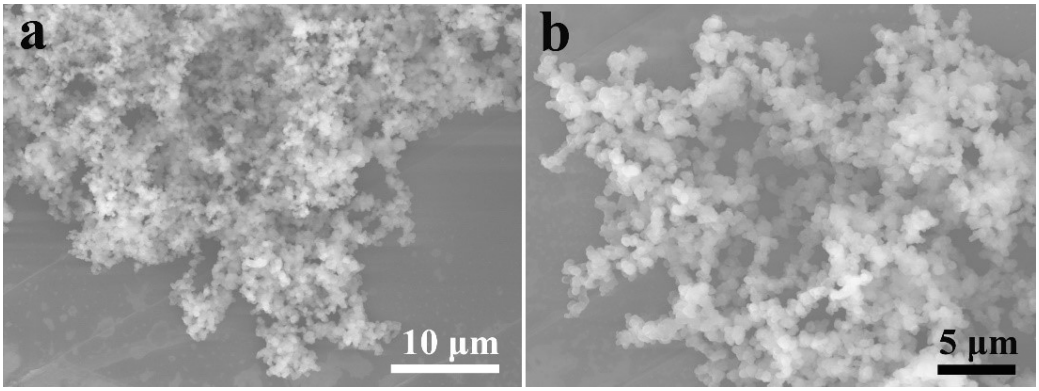

Fig. S3. (a,b) SEM images of COF.

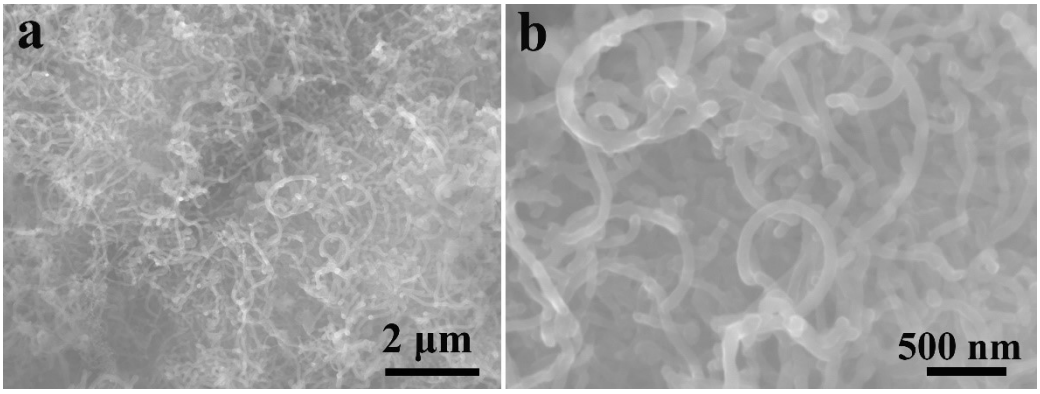

Fig. S4. (a,b) SEM images of CNTs@COF-2.

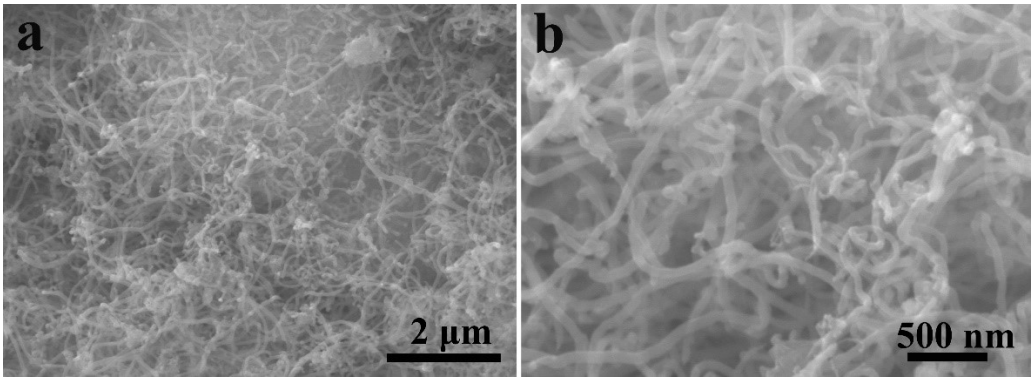

Fig. S5. (a,b) SEM images of CNTs@COF-1.

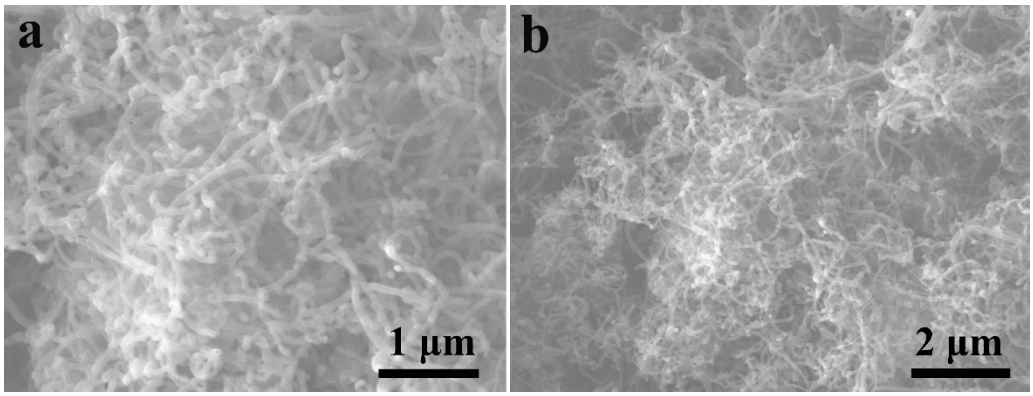

Fig. S6. (a,b) SEM images of CNTs@COF-3.

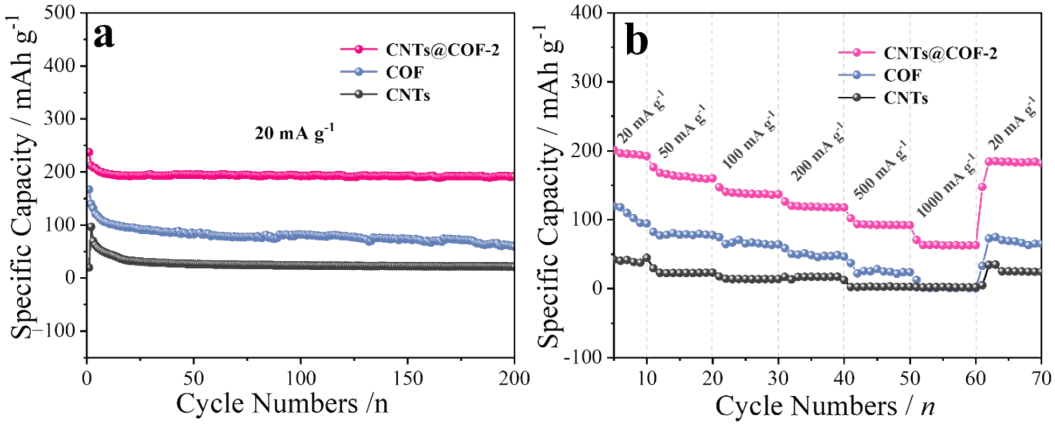

Fig. S7. (a) Cycling performances of CNTs@COF-2, COF, and CNTs at 20 mA g^{-1}. (b) Rate capabilities for CNTs@COF-2, COF, and CNTs for MIBs at different current densities.

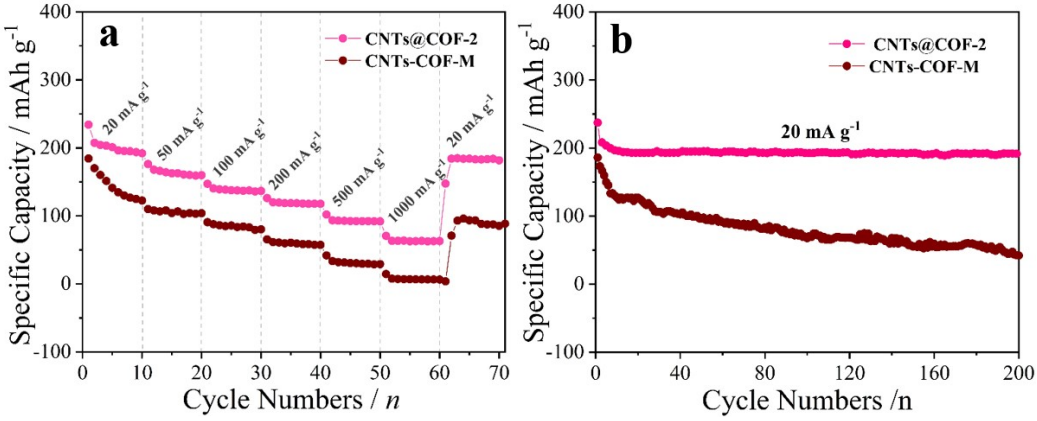

Fig. S8. (a) Rate capabilities for CNTs@COF-2 and CNTs-COF-M for MIBs at different current densities. (b) Cycling performances of CNTs@COF-2 and CNTs-COF-M at 20 mA g^{-1}.

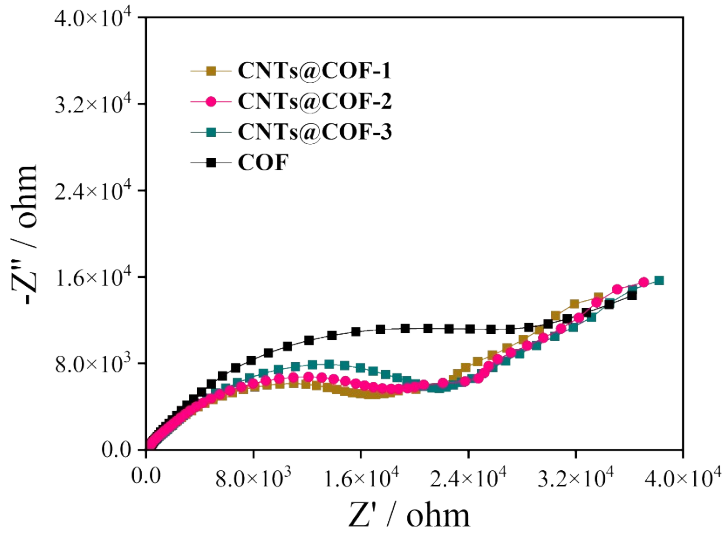

Fig. S9. Nyquist plots of CNTs@COF-1, CNTs@COF-2, CNTs@COF-3, and COF before cycling.

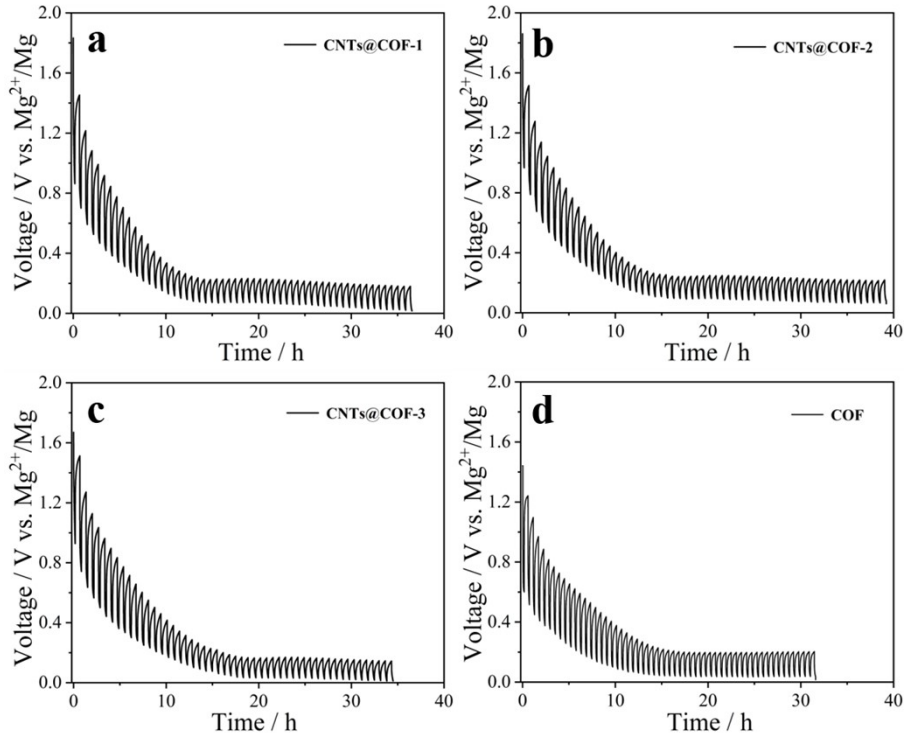

Fig. S10. (a-d) GITT profiles of the discharge process of CNTs@COF-1, CNTs@COF-2, CNTs@COF-3, and COF.

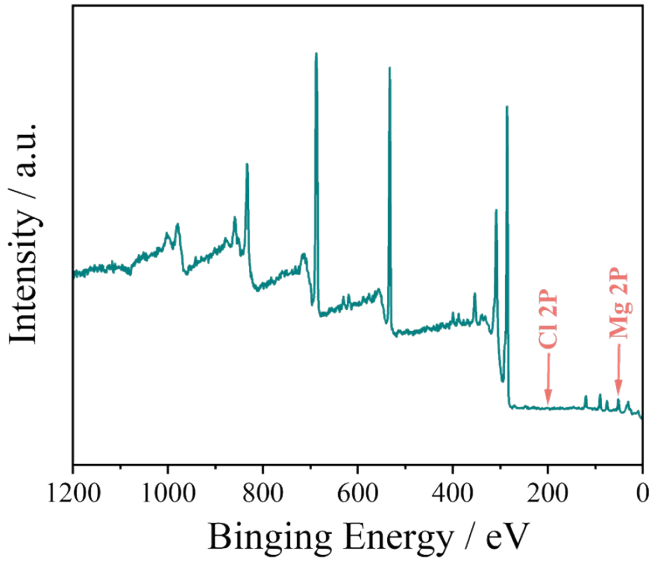

Fig. S11. Survey XPS spectrum of CNTs@COF-2 after the 20th discharge process.

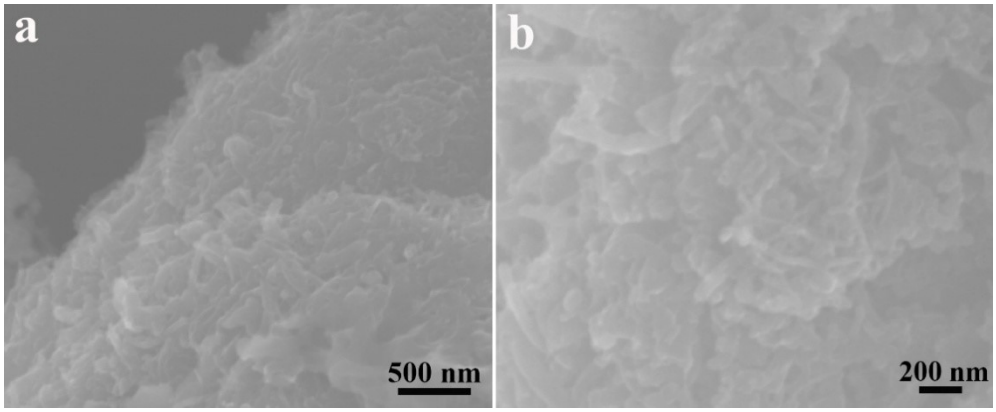

Fig. S12. (a,b) SEM images of CNTs@COF-2 after 200 cycles charge-discharge process.

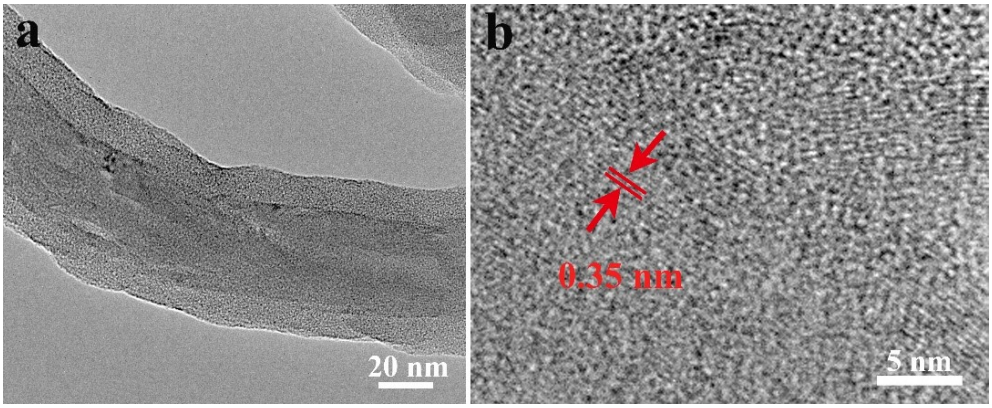

Fig. S13. (a) TEM and (b) HRTEM images of CNTs@COF-2 after 200 cycles charge-discharge process.

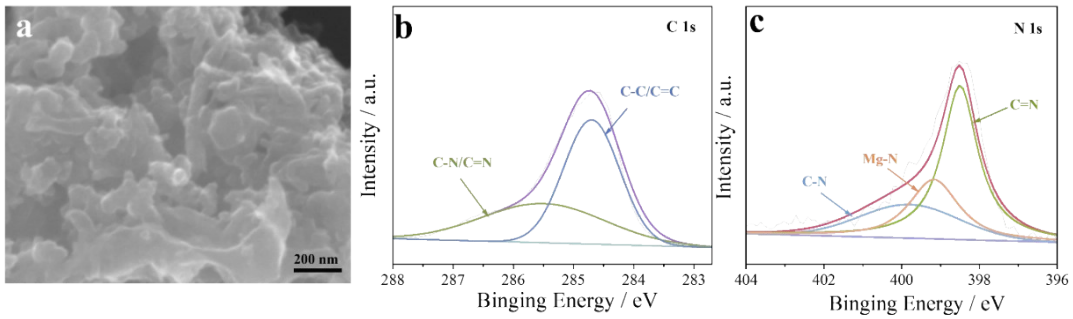

Fig. S14. (a) SEM image and XPS spectra of (b) C1s and (c) N 1s for CNTs@COF-2 after 3000 cycles at 500 mA g^{-1} charge-discharge process.

Table S1. The mass fractions of N and C element in COF, CNTs@COF-1, CNTs@COF-2, and CNTs@COF-3.

Electrodes	N	C
COF	16.2%	83.8%
COF@CNT-1	11.0%	89.0%
COF@CNT-2	6.0%	94.0%
COF@CNT-3	4.5%	95.5%

Table S2. Comparison of electrochemical performance of CNTs@COF-2 with other previously reported cathode materials for MIBs.

Electrode material	**Current Density (mA g^{-1})**	**Reversible capacity (mAh g^{-1})**	**Cycle Numbers (n)**	**Ref.**
CNTs@COF-2	**20**	**191.7**	**200**	**This work**
	500	**107.6**	**3000**	
V_2MoO_8	20	135	50	*Nano Energy 2017, 34, 26*
VO_2	20	154.9	100	*ACS Appl. Mater. Interfaces 2017, 9, 17060*
a-MoS_3@CNT	100	175	50	*Nanoscale 2019, 11, 16043-16051*

SO_2	100	13.8	50	
V_2C MXene	50	~110	480	*Small 2020, 16, 1906076*
Ti_3C_2Tx/CNT	100	~80	500	*ACS Appl. Mater. Interfaces 2017, 9, 4296*
Cu_2Se	26	~110	300	*Electrochim. Acta 2018, 261, 503*
$LiCrTiO_4$	20	~125	30	*Chem. Eur. J. 2017, 23, 17935*
$Li_4Ti_5O_{12}$	60	~125	500	*Angew. Chem. Int. Ed. 2015, 54, 5757*
$Cu_2Mo_6S_8$	4	85	20	*J. Soild State Chem. 2016, 242, 151−154.*
peo-MoS_2	5	74	30	*Nano Lett. 2015, 15, 2194−2202.*
Mn_3O_4	15.4	63	1000	*Chem. Mater. 2016, 28, 6459−6470.*
$K_xMn_8O_{16}$	100	123	20	*Chem. Commun. 2016, 52, 4088−4091.*